Tuning Frictional Properties of Kirigami Altered Graphene Sheets using Molecular Dynamics and Machine Learning

Designing a Negative Friction Coefficient

Mikkel Metzsch Jensen



Thesis submitted for the degree of Master in Computational Science: Materials Science 60 credits

Department of Physics
Faculty of mathematics and natural sciences

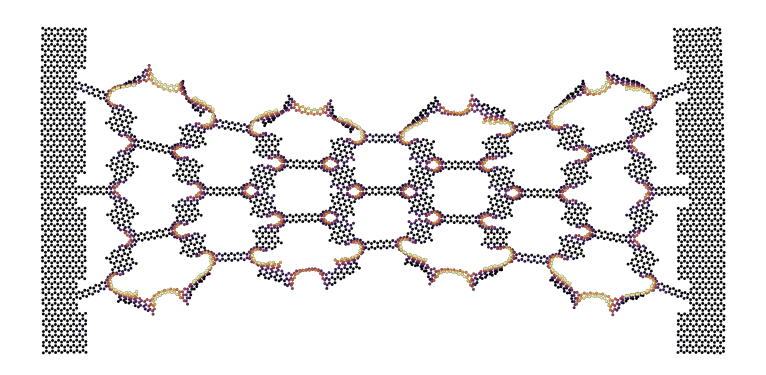
UNIVERSITY OF OSLO

Spring 2023

Tuning Frictional Properties of Kirigami Altered Graphene Sheets using Molecular Dynamics and Machine Learning

Designing a Negative Friction Coefficient

Mikkel Metzsch Jensen





Abstract

Abstract.

Acknowledgments

Acknowledgments.

List of Symbols

 F_N Normal force (normal load)

vi LIST OF SYMBOLS

Acronyms

FFM Friction Force Microscopes. 7

LJ Lennard-Jones. 8

MD Molecular Dynamics. 2, 3, 7, 8

ML Machine Learning. 2, 3

viii Acronyms

Contents

1	ntroduction	1
	.1 Motivation	 1
	.2 Goals	 3
	.3 Contributions	 3
	.4 Thesis structure	 3
Ι	Background Theory	5
2	Molecular Dynamics	7
	2.1 Potentials	
	2.1.1 General formulation of potentials	
	2.1.2 Lennard Jones	 8
	2.1.3 Stillinger weber	
	2.1.4 Tersoff	
	.2 Integration	
	2.2.1 Velocity Verlet	
	3.3 Thermostats	
	2.3.1 Langevin thermostat	
	2.3.2 Implementing Langevin	
	4.4 MD limitations (?)	
	5 LAMMPS	 15
ΙΙ	Simulations	17
Αı	pendices	19
Αı	pendix A	21
_		
Aj	pendix B	23
Αı	pendix C	25

X CONTENTS

Chapter 1

Introduction

Structure of Motivation section:

- 1. Introduce and motivate friction broadly.
- 2. Motives for friction control using a grasping robot as example.
- 3. Analog to gecko feet where adhesive properties are turned on and off.
- 4. Interest in origin of friction through nanoscale studies which further motivates the use of MD.
- 5. Intro to metamaterials and the use of kirigami designs,
- 6. How to optimize kirigami designs with reference to Hanakata and motivating the use of ML.
- 7. Out-of-plane buckling motivates the use of kirigami for frictional properties.

Does some of the latter paragraphs belong to the approach section?

1.1 Motivation

Friction is a fundamental force that takes part in most of all interactions with physical matter. Even though the everyday person might not be familiar with the term friction we recognize it as the inherent resistance to sliding motion. Some surfaces appear slippery and some rough, and we know intuitively that sliding down a snow covered hill is much more exciting than its grassy counterpart. Without friction, it would not be possible to walk across a flat surface, lean against the wall without falling over or secure an object by the use of nails or screws [p. 5] [1]. It is probably safe to say that the concept of friction is integrated in our everyday life to such an extent that most people take it for granted. However, the efforts to control friction dates back to the early civilization (3500 B.C.) with the use of the wheel and lubricants to reduce friction in translational motion [2]. Today, friction is considered a part of the wider field tribology derived from the Greek word Tribos meaning "rubbing" and includes the science of friction, wear and lubrication [2]. The most compelling motivation to study tribology is ultimately to gain full control of friction and wear for various technical applications. Especially, reducing friction is of great interest as this has tremendous advantages for energy effeciency. It has been reported that tribological problems have a significant potential for economic and environmental improvements [3]:

"On global scale, these savings would amount to 1.4% of the GDP annually and 8.7% of the total energy consumption in the long term." [4].

On the other hand, the reduction of friction is not the only sensible application for tribological studies. Controlling frictional properties, besides minimization, might be of interest in the development of a grasping robot where a finetuned object handling is required. While achieving a certain "constant" friction response is readily obtained through appropriate material choices during manufacturing, we are yet to unlock the capabilities to alter friction dynamically on the go. One example from nature inspiring us to think along theese lines are the gecko feet. More precisely, the Tokay gecko has recieved a lot of attention in scientific studies aiming to unravel the underlying

mechanism of its "togglable" adhesion properties. Although geckos are able to produce large adhesive forces, they retain the ability to remove their feet from an attachment surface at will [5]. This makes the gecko able to achieve a high adhesion on the feet when climbing a vertical surface while lifting it for the next step remains reletively effortless. For a grasping robot we might consider an analog frictional concept of a surface material that can change from slippery to rough on demand depending on specific tasks.

In the recent years an increasing amount of interest has gone into the studies of the microscopic origin of friction, due to the increased possibilities in surface preparation and the development of nanoscale experimental methods. Nano-friction is also of great concern for the field of nano-machining where the frictional properties between the tool and the workpiece dictates machining characteristics [3]. With concurrent progress in computational power and devolopment of Molecular Dynamics (MD), numerical investigations serve as an extremely useful tool for getting insight into the nanoscale mechanics associated with friction. This simulation based approach can be considered as a "numerical experiment" enabling us to create and probe a variety of high complexity systems which are still out of reach for modern experimental methods.

In materials science such MD-based numerical studies have been used to explore the concept of so-called metamaterials where material compositions are designed meticulously to enhance certain physical properties [6][7][8][9][10][11]. This is often achieved either by intertwining different material types or removing certain regions completely. In recent papers by Hanakata et al. [6](2018) [7](2020) numerical studies have showcased that mechanical properties of a graphene sheet, in this case yield stress and yield strain, can be altered through the introduction of so-called kirigami inspired cuts into the sheet. Kirigami is a variation of origami where the paper is cut additionally to being folded. While these methods originate as an art form, aiming to produce various artistic objects, they have proven to be applicable in a wide range of fields such as optics, physics, biology, chemistry and engineering [12]. Various forms of stimuli enable direct 2D to 3D transformations through folding, bending, and twisting of microstructures. While original human designs have contributed to specific scientiffic applications in the past, the future of this field is highly driven by the question of how to generate new designs optimized for certain physical properties. However, the complexity of such systems and the associated design space makes for seemingly intractable problems ruling out analytic solutions.

Earlier architecture design approaches such as bioinspiration, looking at gecko feet for instance, and Edisonian, based on trial and error, generally rely on prioir knowdelegde and an experienced designer [9]. While the Edisonian approach is certainly more feasible through numerical studies than real world experiments, the number of combinations in the design space rather quickly becomes too large for a systematic search, even when considering the simulation time on modern day hardware. However, this computational time constraint can be relaxed by the use of machine learning (ML) which have proven successful in the establishment of a mapping from the design space to physical properties of interest. This gives rise to two new styles of design approaches: One, by utilizing the prediction from a trained network we can skip the MD simulations all together resulting in an accelerated search of designs. This can be further improved by guiding the search accordingly to the most promising candidates, as for instance done with the genetic algorithm which suggest new designs based on mutation and crossing of the best candidates so far. Another, even more sophisticated approach, is through generative methods such as Generative Adversarial Networks (GAN). By working with a so-called encoder-decoder network structure, one can build a model that reverses the prediction process. That is, the model predicts a design from a set of physical target properties. In the papers by Hanakata et al. both the accelerated search and the inverse design approach was proven successful to create novel metamaterial kirigami designs with the graphene sheet.

Hanakata et al. attributes the variety in yield properties to the non-linear effects arrising from the out-of-plane buckling of the sheet. Since it is generally accepted that the surface roughness is of great importance for frictional properties it can be hypothesized that the kirigami cut and stretch procedure can also be exploited for the design of frictional metamaterials. For certain designs we might hope to find a relationship between stretching of the sheet and frictional properties. If significiant, this could give rise to a variability of the friction reponse beyond manufacturing material choice. For instance, the grasping robot might apply such a material as artifical skin for which stretching or relaxing of the surface could result in a changeable friction strength; Slippery and smooth when in contact with people and rough and firmly gripping when moving heavy objects. In addition, a possible coupling between stretch and the normal load through a nanomachine design would allow for an altered friction coefficient. This invites the idea of non-linear friction coefficients which might in theory also take on negative values given the right response from stretching. The latter would constitute an extremely rare property. This has (only?) been reported indirectly for bulk graphite by Deng et al. [13] where the friction kept increasing during the unloading phase. Check for other cases and what I can really say here.

1.2. GOALS 3

To the best of our knowledge, kirigami has not yet been implemented to alter the frictional properties of a nanoscale system. In a recent paper by Liefferink et al. [14](2021) it is reported that macroscale kirigami can be used to dynamically control the macroscale roughness of a surface through stretching which was used to change the frictional coefficient by more than one order of magnitude. This support the idea that kirigami designs can in fact be used to alter friction, but we believe that taking this concept to the nanoscale regime would envolve a different set of underlying mechanisms and thus contribute to new insight in this field.

1.2 Goals

In this thesis we investigate the possibility to alter and control the frictional properties of a graphene sheet through application of kirigami inspired cuts and stretching of the sheet. With the use of MD simulations we evaluate the friction properties under different physical conditions in order to get insight into the prospects of this field. By evaluating variations of two kirigami inspired patterns and a series of random walk generated patterns we create a dataset containing information of the frictional properties associated with each design under different load and stretch conditions. We apply ML to the dataset and use an accelerated search approach to optimize for different properties of interest. The subtask of the thesis are presented more comprehensively in the following.

- 1. Define a sheet indexing that allows for an unquie mapping of patterns between a hexagonal graphene lattice representation to a matrix representation suited for numerical analysis.
- 2. Design a MD simulation procedure to evaluate the frictional properties of a given graphene sheet under specified physical conditions such as load, stretch, temperature etc.
- 3. Find and implement suitable kirigami patterns which exhibit out-of-plane buckling under tensile load. This includes the creation of a framework for creating variations within each pattern class. Additionally create a procedure for generating different styles of random walk patterns.
- 4. Perform a pilot study of a representative subset of patterns in order to determine appropriate simulation parameters to use for the further study along with an analysis of the frictional properties shown in the subset.
- Create a dataset consisting of the chosen kirigami variations and random walk patterns and analyse data trends.
- 6. Train a neural network to map from the design space to physical properties such as mean friction, maximum friction, contact area etc. and evaluate the performance.
- 7. Perform an accelerated search optimizing for interesting frictional properties using the ML model. This should be done both through the pattern generation procedures and by following a genetic algorithm approach.
- 8. Use the most promising candidtes from the accelerated search to investigate the prospects of creating a nanomachine setup which exhibits a negative friction coefficient.
- 9. Study certain designs of interest with the scope of revealing underling mechanism. This includes simple correlation analysis but also a visualization of feature and gradient maps of the ML network.

Is the list of subtask to specific? Some of the details here might be better suited for the thesis structure section.

1.3 Contributions

What did I actually achieve

1.4 Thesis structure

How is the thesis structured.

Part I Background Theory

Chapter 2

Molecular Dynamics

Molecular Dynamics (MD) is an atomistic simulation method which are a popular and powerful for the investigation of atomic scale friction due to the ability to track every single atom in a system [15]. Thanks to the advances in computing algorithms and hardware the recent years has witnessed a remarkable increase in our ability to similate tribological system [16]. We are going to use MD as our main numerical approach in order to simulate and investigate the effect of nanoscale kirigami on our system. Such small scale modifications are still out of reach for experimental approaches while on the other hand the complexity of the system rules the possibility of using analytical solutions. This is why atomistic simulations like MD is one of few great choices to tackle this problem. Other alternatives like Ab inito methods, which calculate the interaction based on quantam mechanis Check up on thisd and get source, gives more detailed results but comes with a higher computational cost. MD simulations are already being limited for its ability to capture larger-scale features such as time and large masses, which will only increase with choices of more detailed methods. [15]. Thus, the weaknesses include the lack of quantum effects.

A MD simulation can be considered as a computational "experiment". Given a set of inital conditions and a mathematically defined model for interatomic forces based on relative positions, we can solve Newton's equation of motion by numerical integration [17, p. 303]. Thus the interatomic forces are derived from interparticle interaction potentials, which is the heart of MD simulations and the specific choice of potentials can often be quite challenging. Even though most potentials can be parameterized to fit a given material, some potentials are better suited for different kind of materials due to an attention in a variety of materialistic properties and mechanics source.

2.1 Potentials

The potentials used in a MD simulations plays a major role for the obtained results. In fact development and analysis of the effect on potentials in MD is a whole field in itself source? In this thesis, we will not be carying out an extensive analysis for the potential choice as this rather quickly becomes too extensive. Instead, we consult with the litterature on similar MD frictional studies in the search for a set of potentials that have been proven to produce reasonible result. However, we note that this immediately makes room for an extended study of the results to come regarding the dependency of specific potential choices. For the choice of potentials, and materials, we take a basis in the numerical MD study by Li et al. [18] simulating a FFM type setup where a Si tip indents a graphene sheet supported by a Si substrate. It obiously differs from our system by the fact that we intent to drag the whole sheet rather than indenting it with a tip, but in the scope of choosing the potential setup this should be a appropriate starting point. The covalent bonds of C-C in graphene and Si-Si in the substrate is described by the Tersoff and Stillinger-Weber potentials, respectively. A typical 12-6 Lennard-Jones potential is used to describe the van der Waals adhesive interaction between graphene and the substrate.

2.1.1 General formulation of potentials

The physical potential governing the mechanics of the atomic system can generally be thought of as an the n-body expansion in orders of participating atoms as

$$E = \sum_{i} V_1(\mathbf{r}_i) + \sum_{\substack{i,j\\i < j}} V_2(\mathbf{r}_i, \mathbf{r}_j) + \sum_{\substack{i,j,k\\i < j < k}} V_3(\mathbf{r}_i, \mathbf{r}_j, \mathbf{r}_i) + \cdots,$$

where \mathbf{r}_n is the position of the *n*th particle and V_m is called an *m*-body potential [19]. The first one-body term corresponds to an external potential (e.g. gravity), followed by the two-body term, the three-body term and so on. The simplest model that includes particle interaction is the pair potential truncating the expansion after the two-body term. A general feature of the pair potentials is that they favor close-packed structures which is unsuited to describe covalent bonds that take more open structures. In particular, pair potentials are completely inapplicable to strongly covalent systems [19]. In order to accommodate the description of covalent bonds the natural step is thus to include the next step of the expansion, the three-body terms, as we will use for the modeling of the C-C bonds in the graphene sheet and the Si-Si bonds in the Silicon substrate. For the interaction between the sheet and the substrate we use a Lennard Jones pair potential describing the non-bonded van der Waals interaction which has come to be the standard way to treat intermaterial interactions in friction simulations [3, 20–22]. I can put more sources here

In the following we introduce the potentials in a more formal way.

2.1.2 Lennard Jones

TODO: Add potential curve figure

The theoretical basis in this subsection is based on [23–25].

The Lennard-Jones (LJ) model is probably one of the most commonly used pair potentials for MD simulations. LJ models the potential energy between two non-bonding atoms solely based on interatomic distance. The model accounts for attractive forces arising from dipole-dipole, dipole-induced dipole and London interactions, and repulsive forces that capture the hard core of overlapping wave functions at small distances (double check this statement). Thus, it assummes neutrally charged atoms and was originally proposed for noble gases. The classical 12-6 version of the model, referring to the powers of the repulsive and attractive forces respectively, reads

$$E = 4\epsilon \left[\left(\frac{\sigma}{r} \right)^{12} - \left(\frac{\sigma}{r} \right)^{6} \right], \qquad r < r_c, \tag{2.1}$$

where r is the interatomic distance with cut-off r_c , ϵ is the depth of the potential well and σ the interatomic distance where the potential is zero. By solving for the potential minimum (dE/dr = 0) we find the equilibrium distance to be $r_0 = \sigma 2^{1/6}$. This makes for a slightly more intuitive interpration of σ as the parameter which sets the equilibrium distance between atoms, i.e. the dividing line for which the force is repulsive or attractive.

Refer to choosen parameters.

2.1.3 Stillinger weber

TODO: Add potential figure and or figure illustrating three body angles.

The theoretical background of this subsection is based on [[26], [27]]

The stillinger weber potential takes the form of a three body potential

$$E = \sum_{i} \sum_{j>i} \phi_2(r_{ij}) + \sum_{i} \sum_{j\neq i} \sum_{k>j} \phi_3(r_{ij}, r_{ik}, \theta_{ijk}),$$

where r_{ij} denotes the distance between atom i and j, and θ_{ijk} the angle between bond ij and jk. The summations is over all neighbours j and k of atom i within a cut-off distance $r = a\sigma$.

The two-body term ϕ_2 builds from the LJ model with the addition of an exponetial cutoff term

$$\phi_2(r_{ij}) = A_{ij}\epsilon_{ij} \left[B_{ij} \left(\frac{\sigma_{ij}}{r_{ij}} \right)^{p_{ij}} - \left(\frac{\sigma_{ij}}{r_{ij}} \right)^{q_{ij}} \right] \exp\left(\frac{\sigma_{ij}}{r_{ij} - a_{ij}\sigma_{ij}} \right). \tag{2.2}$$

2.1. POTENTIALS 9

The model parameters A, ϵ , B, σ , p, q and a comes with i,j indices to indicate that theese parameters should be specified for each unique pair of atom types. However, in our case we will only provide a single value for each model parameter as we are exclusively dealing with Si-Si bonds. We see that the first term in Eq. (2.2) is reminiscent of the LJ model in Eq. (2.1) while the last term effectively drives the potential to zero at $r = a\sigma$, which is the chosen cut-off distance for the potential evaluation. With the model parameters for the Si-Si modelling (see Table 2.1) the cut-off becomes ~ 3.8 Å. The three body term includes an angle dependency as

$$\phi_3(r_{ij}, r_{ik}, \theta_{ijk}) = \lambda_{ijk} \, \epsilon_{ijk} \left[\cos \theta_{ijk} - \cos \theta_{0,ijk} \right]^2 \exp\left(\frac{\gamma_{ij}\sigma_{ij}}{r_{ij} - a_{ij}\sigma_{ij}}\right) \exp\left(\frac{\gamma_{ik}\sigma_{ik}}{r_{ik} - a_{ik}\sigma_{ik}}\right), \tag{2.3}$$

where $\theta_{0,ijk}$ is the equilibrium angle. The first term of Eq. (2.3) includes an angle dependency analog to a harmonic oscillator based on a cosine angle distance from the equilibrium angle. The final two terms act again as a cut-off function by driving the potential to zero at $r_{ij} = a_{ij}\sigma_{ij}$ and $r_{ik} = a_{ik}\sigma_{ik}$ respectively. We adopt the parameters for Si-Si suggested in the original paper by Stillinger and Weber [27] which is shown in Table 2.1 along with an interpretation of each model parameter.

Table 2.1: Parameters for the stilliner weber potential used for intermolecular interactions in the silicon substrate. The parameters are adopted from [27].

Parameter	Value	Description	
ϵ	2.1683	Individual depth of the potential well for each pair and	
		triplets of atom types.	
σ.	2.0951	Distance for which the individual pair interactions has zero	
σ		potential (analog to the LJ model).	
a	1.80	The individual cut-off distance for each pair of atom types.	
λ	21.0	The overall depth of the three-body potential well.	
γ	1.20	The shape of the three-body cut-off terms.	
$\cos\left(\theta_{0}\right)$	-1/3	Cosine of equilibrium angle.	
A	7.049556277	The overall depth of the two-body potential well.	
В	0.6022245584	Scales the repulsion part of the two-body term.	
m	4.0	The power dependency for the repulsion part of the	
p		two-body term.	
a	0.0	The power dependency for the attraction part of the	
q		two-body term.	
	0.0	(LAMMPS specific) Option to define a different cut-off	
tol		than the theoretical $r = a\sigma$. $tol = 0$ refers to the use of the	
		theoretical.	

2.1.4 Tersoff

This theoretical background in this subsection is based on [19, 28].

The Tersoff potential abandon the idea of a general *n*-body form and attempts instead to build the model on a more physics informed approach; The more neighbours an atom has the weaker the bonds will be. Thus it introduces the bond order (bond strentgh), that is environment specific and decrease with increasing bond coordination (number of neighbours for a given atom). The potential energy is taken to have the form

$$E = \sum_{i} E_i = \frac{1}{2} \sum_{i \neq j} V_{ij},$$

$$V_{ij} = f_C(r_{ij}) \left[f_R(r_{ij}) + b_{ij} f_A(r_{ij}) \right],$$

where the total potential energy E is decomposed into a bond energy V_{ij} . The indices i and j run over the atoms of the system with r_{ij} denoting the distance between atom i and j. Notice that the sum includes all combinations of i, j but $i \neq j$, meaning that an atom cannot bond to itself, but we do count other bonds twice, e.g. ((1,2) and (2,1)), which is the explanation for the additional factor 1/2. The reasoning behind comes from the asymmetry of the bond order $b_{ij} \neq b_{ji}$ leading to a $V_{ij} \neq V_{ji}$. The bond energy is composed of a repulsive

term f_R , arising from overlapping wave functions, and an attractive term f_A associated with bonding. f_C is simply a smooth cut-off function to increase computational efficiency. b_{ij} represent the bond order, i.e. the strength of the bonds, which depends inversely on the number of bonds, the bond angles (θ_{ijk}) and optionally the relative bonds lengths (r_{ij}, r_{jk}) . Notice that an additional cut-off term a_{ij} was originally multiplied to f_R as a way of including terms that limit the range of the interactions to the first neighbour shell. This kind of limitation is already included in b_{ij} for the attractive term f_A but is often omitted for the repulsive term f_R , and we do so to by setting $a_{ij} = 1$.

The cut-off function f_C goes from 1 to 0 over a small interval range $R \pm D$ as

$$f_C(r) = \begin{cases} 1 & r < R - D \\ \frac{1}{2} - \frac{1}{2}\sin\left(\frac{\pi}{2}\frac{r - R}{D}\right) & R - D < r < R + D \\ 0 & r > R + D \end{cases}$$

which is continuous and differentiable for all r. R is usually chosen to include only the first neighbour shell. The repulsive and attractive terms f_R and f_A is modelled as an exponetial function, similar to a morse potential,

$$f_R(r) = A \exp(-\lambda_1 r),$$

$$f_A(r) = -B \exp(-\lambda_2 r).$$

The novel feature of the Tersoff model lies in modeling of the bond order b_{ij} which includes three-body interactions by summing over a third atom $k \neq i, j$ within the cut-off $r_{ik} < R + D$ as shown in the following.

$$b_{ij} = \left(1 + \beta^n \zeta_{ij}^n\right)^{-\frac{1}{2n}} \tag{2.4}$$

$$\zeta_{ij} = \sum_{k \neq i,j} f_C(r_{ik}) g\left(\theta_{ijk} \left(r_{ij}, r_{ik}\right)\right) \exp\left(\lambda_3^m \left(r_{ij} - r_{ik}\right)^m\right)$$
(2.5)

$$g(\theta) = \gamma_{ijk} \left(1 + \frac{c^2}{d^2} - \frac{c^2}{\left[d^2 + (\cos \theta - \cos \theta_0)^2 \right]} \right).$$
 (2.6)

In Eq. (2.6) $\zeta_{i,j}$ is an effective coordination and $g(\theta)$ captures angle dependency as it is minimized at the equilibrium angle $\theta = \theta_0$. The parameters used to model the graphene C-C bonds is adopted from J. Tersoff [29] and summarized in Table 2.2

Table 2.2: Parameters for the tersoff potential used for intermolecular interations in the graphene sheet

Parameter	Value	Description		
R	1.95 Å	Center distance for cut-off.		
D	0.15 Å	Thickness of cut-off region.		
λ_1	3.4879 Å^{-1}	Decay of repulsion potential term f_R .		
λ_2	2.2119 Å^{-1}	Decay of attractive potential term f_A .		
A	1393.6 eV	Repulsion potential maximum at the core $(f_R(r_{ij}=0))$.		
B	346.74 eV	Attractive potential minimum at core $(f_A(r_{ij}=0))$.		
β	1.5724×10^{-7}	Base for the exponetial scaling of the effective coordination		
		effect on bond strength b_{ij} .		
n	0.72751	Power law exponent for the bond order dependency.		
λ_3	$0.0 \ {\rm \AA}^{-1}$	Base for the exponential cut-off of the effective		
^3		coordination $\zeta_{i,j}$.		
m	_	Exponent for the exponential cut-off of the effective		
116		coordination $\zeta_{i,j}$. Not relevant since $\lambda_3 = 0$.		
γ	1.0	Linear scaling of the angle dependency term.		
c	3.8049×10^4	Strength of the angular effect.		
d	4.3484	Determines the "sharpness" of the angular dependency.		
$\cos\left(\theta_{0}\right)$	-0.57058	Cosine of the equilibrium angle.		

2.2. INTEGRATION 11

2.2 Integration

Assuming that one has defined a system of particles, setting the atom types, initial positions and velocties, and interartomic potentials, we need to move the system forward in time. By solving Newtons equations of motion we achieve this by effectively sampling the microcanonical ensemble characterized by a constant number of particles N, volume V and energy E, hence denoted NVE. Newtons equations of motion read

$$m_i \frac{d^2 \mathbf{r}_i}{dt^2} = \mathbf{F}_i = -\nabla U_i, \tag{2.7}$$

where i is the particle index, m_i its mass, $\mathbf{r}_i = (x_i, y_i, z_i)$ the position, t is time, $\nabla_i = (\frac{\partial}{\partial x_i}, \frac{\partial}{\partial y_i}, \frac{\partial}{\partial z_i})$ and U_i the potential energy. The potential energy is defined by the interatomic potentials and any external forces applied to the system. Since the forces defined by the potentials is conservative we expect the energy of the solution to be conserved. We can redefine Eq. (2.7) in terms of two coupled first order differential equations

$$\dot{\mathbf{v}}_i(t) = \frac{\mathbf{F}}{m_i}, \qquad \dot{\mathbf{r}}_i(t) = \mathbf{v}_i(t), \tag{2.8}$$

where $\dot{x} = dx/dt$ is Newton's notation for the time derivative and $\mathbf{v} = (v_x, v_y, v_z)$ is velocity. Numerically we can solve the coupled equations by integrating over discrete timnesteps. That is, we discretize the solution into temporal steps $t_k = t_0 + k\Delta t$ with start time t_0 and time-step Δt .

2.2.1 Velocity Verlet

A popular approach to the numerical integration of Newtons equations of motion, when written as two coupled first order differential equations Eq. (2.8), is the *velocity verlet* algorithm. We can derive the algorithm by the use of Taylor expansions. We begin by expanding the next-step position vector $\mathbf{r}_i(t + \Delta t)$ at time t

$$\mathbf{r}_{i}(t+\Delta t) = \mathbf{r}_{i}(t) + \dot{\mathbf{r}}_{i}(t)\Delta t + \frac{\ddot{\mathbf{r}}_{i}(t)}{2}\Delta t^{2} + \mathcal{O}(\Delta t^{3}), \tag{2.9}$$

where $\ddot{\mathbf{r}} = d^2\mathbf{r}/dt^2$ and Δt^n is simply the relaxed notation for $(\Delta t)^n$. Thus, the remaining $\mathcal{O}(\Delta t^3)$ term is big O notation for the truncation including a dependence of Δt^3 and higher order. Similarly, we take the expansions of the next-step velocity vector $\mathbf{v}_i(t + \Delta t)$ at time t

$$\mathbf{v}_i(t+\Delta t) = \mathbf{v}_i(t) + \dot{\mathbf{v}}_i(t)\Delta t + \frac{\ddot{\mathbf{v}}_i(t)}{2}\Delta t^2 + \mathcal{O}(\Delta t^3). \tag{2.10}$$

Finnally, by taking the expansion of $\dot{\mathbf{v}}_i(t+\Delta t)$ we can eliminate the $\ddot{\mathbf{v}}_i$ -term in Eq. (2.10) and simplify it as shown in the following.

$$\dot{\mathbf{v}}_{i}(t + \Delta t) = \dot{\mathbf{v}}_{i}(t) + \ddot{\mathbf{v}}_{i}(t)\Delta t + \mathcal{O}(\Delta t^{2})$$

$$\frac{\ddot{\mathbf{v}}_{i}(t)}{2}\Delta t^{2} = \frac{\Delta t}{2} \left(\dot{\mathbf{v}}(t + \Delta t) - \dot{\mathbf{v}}_{i}(t)\right) + \mathcal{O}(\Delta t^{3})$$

$$\downarrow$$

$$\mathbf{v}_{i}(t + \Delta t) = \mathbf{v}_{i}(t) + \dot{\mathbf{v}}_{i}(t)\Delta t + \frac{\Delta t}{2} \left(\dot{\mathbf{v}}_{i}(t + \Delta t) - \dot{\mathbf{v}}_{i}(t)\right) + \mathcal{O}(\Delta t^{3})$$

$$= \mathbf{v}_{i}(t) + \frac{\Delta t}{2} \left(\dot{\mathbf{v}}_{i}(t) + \dot{\mathbf{v}}_{i}(t + \Delta t)\right) + \mathcal{O}(\Delta t^{3}).$$
(2.11)

By combining Eq. (2.9) and Eq. (2.11), and $\dot{\mathbf{v}} = \mathbf{F}_i(t)/m_i$ and $\mathbf{v} = \dot{\mathbf{r}}$ we arrive at the final scheme

$$\mathbf{r}_{i}(t + \Delta t) = \mathbf{r}_{i}(t) + \mathbf{v}_{i}(t)\Delta t + \frac{\mathbf{F}_{i}(t)}{2m_{i}}\Delta t^{2} + \mathcal{O}(\Delta t^{3}),$$

$$\mathbf{v}_{i}(t + \Delta t) = \mathbf{v}_{i}(t) + \frac{\mathbf{F}_{i}(t) + \mathbf{F}_{i}(t + \Delta t)}{2m_{i}}\Delta t + \mathcal{O}(\Delta t^{3}).$$

This scheme will give a local error on the order Δt^3 corresponding to a global error of Δt^2 . One of the most popular ways to implement this numerically is as stated in the following steps.

- 1. Calculate $v_{k+\frac{1}{2}} = v_k + \frac{F_k}{2m} \Delta t$.
- 2. Calculate $r_{k+1} = r_k + v_{k+\frac{1}{2}} \Delta t$.
- 3. Evaluate the force $F_{k+1} = F(r_{k+1})$.
- 4. Calculate $v_{k+1} = v_{k+\frac{1}{2}} + \frac{F_{k+1}}{2m} \Delta t$

2.3 Thermostats

As we already mentioned above in Sec. 2, any kind of sliding friction involves mechanical work, some of which is then transformed into heat (the rest going into structural transformations, wear, etc.). The heat is then transported away by phonons (and electrons in the case of metallic sliders) and eventually dissipated to the environment [16].

Likewise all excitations generated in the simulations should be allowed to propagate in the system and disperses in the bulk of both sheet and substrate. Due to small simulation size theese is likely to relfect back and ''pile up" unphysically Thus in order to avoid continuous heating and attain a steady state the (Joule) heat must be removed at a steady state. This is very the viscous damping of the langevin equations enter the picture. It can be difficult to set the value γ for the magnitude of this damping. The unphysical introduction of heat sink can be mittigated by some modifictions he mention, which is kind of next level I guess.

2.3.1 Langevin thermostat

In order to control the temperature of the system we introduce the so-called Langevin thermostat. This is a stochastic thermostat that modifies Newtons equation of motion such that solution lies in the canonical ensemble characterized by a constant number of particles N, constant volume V and constant temperature T, hence denoted NVT. The canonical ensemble system is represented by the finite system being in contact with an infinite heat bath of temperature T. The NVT ensemble is equivalent to sampling a system in theromodynamic equilibrium where the weight of each microscopic state is given by the boltzmann factor $\exp[-E/(k_BT)]$.

The Langevin equation is the modified version of Newtons second law for a Brownian particle. A brownian particle is a small particle suspendend in liquid, e.g. pollen or dust, named after Robert brown (1773–1858) who was the first to observe its jittery motion. The Langevin equation describes this motion as the combination of viscous drag force $-\gamma \mathbf{v}$, where γ is a positive friction coefficient and \mathbf{v} the velocity vector, and a random fluctuation force \mathbf{R} . The langevin equation reads

$$m\frac{d\mathbf{v}}{dt} = -\gamma\mathbf{v} + \mathbf{R} \tag{2.12}$$

where m is the particle mass. This effectively describes the particle of interest, the brownian particle, as being suspendend in a sea of smaller particles. The collision with these smaller particles is modelled by the drag force and the fluctuation force. We notice that if the fluctuation force is excluded Eq. (2.12) becomes

$$m\frac{d\mathbf{v}}{dt} = -\gamma\mathbf{v} \quad \Rightarrow \quad \mathbf{v}_i(t) = v(0)e^{-\frac{\gamma t}{m}},$$

where the solution shows that the brownian particle will come to a complete stop after a long time $\mathbf{v}_i(t \to \infty) \to \mathbf{0}$. This is in violation with the equipartion theorem

$$\frac{1}{2}m\langle v^2\rangle_{eq} = \frac{k_B T}{2},$$

and hence the fluctuation force is nessecary to obtain the correct equilibrium.

The following calculations are done in one dimension in order to simplify the notation. We describe the statistical nature of the collisions as a sum of independent momentum transfers

$$\Delta P = \sum_{i}^{N} \delta p_{i}$$

2.3. THERMOSTATS

where ΔP denotes the change of momentum after N momentum transfers δp_i from the environment to the brownian particle. We assume the first and second moments $\langle \delta p \rangle = 0$ and $\langle \delta p \rangle = \sigma^2$. When N is large the central limit theorem states that the random variable ΔP has a gaussian distribution with $\langle P \rangle = 0$ and $\langle \Delta P^2 \rangle = N \sigma^2$. If we consider the momentum change ΔP over a discrete time Δt , where the number of collisiosn is proportional to time $N \propto \Delta t$, the corresponding fluctuation force $R = \Delta P/\Delta t$ will have a variance

$$\langle R^2 \rangle = \frac{\langle \Delta P^2 \rangle}{\Delta t^2} = \frac{N\sigma^2}{\Delta t^2} \propto \frac{1}{\Delta t}.$$

In a computer simulation we need to pick a random force R(t) from a Gaussian distribution every time-step Δt . These forces will not be correlated as long as Δt is larger than the correlation time of the forces from the molecules which we will assume for this model (I think there exist corrections for this to refer to here). With this assumption we can write the correlation function as

$$\langle R(t)R(0)\rangle = \begin{cases} \frac{a}{\Delta t}, & |\Delta t| < \Delta t/2\\ 0, & |\Delta t| > \Delta t/2, \end{cases}$$
(2.13)

where a is some strength of (...?). In the limit $\Delta t \to 0$ the correlation function becomes

$$\langle R(t)R(0)\rangle = a\delta(t),\tag{2.14}$$

where δ denotes the dirac delta function. This is valid for all spatial coordinates which will all be independent of each other. Since both the drag force and the fluctuation force originate from the molecular fluid, where the drag force $-\alpha \mathbf{v}$ is velocity dependent it is reasonible to assume that fluctuation force is independent of velocity, i.e. $\langle R_i v_j \rangle = 0$ for all cartesian indices i and j.

In the following we will attempt justify the Langevin equaiton (why it is like it is) and determine the relationship between the drag coefficient γ and the random force R.

From the Langevin equation Eq. (2.12) we can compute the velocity autocorrelation function (Move to appendix?). We do this in one dimension for simplicity. We begin by multiplying by $(e^{\gamma t/m})/m$

$$\dot{v}(t)e^{\gamma t/m} + \frac{\gamma}{m}v(t)e^{\frac{\gamma t}{m}} = \frac{F}{m}e^{\frac{\gamma t}{m}},$$

and integrate from $t = -\infty$. By the use of integration by parts on the latter term on the left hand side we calculate the velocity

$$\int_{-\infty}^{t} dt' \ \dot{v}(t') e^{\frac{\gamma t'}{m}} + \frac{\gamma}{m} v(t) e^{\frac{\gamma t'}{m}} = \int_{-\infty}^{t} dt' \ e^{\frac{\gamma t'}{m}} \frac{F(t')}{m}$$

$$\int_{-\infty}^{t} dt' \ \dot{v}(t') e^{\frac{\gamma t'}{m}} + \left(\left[v(t') e^{\frac{\gamma t'}{m}} \right]_{-\infty}^{t} - \int_{-\infty}^{t} dt' \ \dot{v}(t') e^{\frac{\gamma t'}{m}} \right) = \int_{-\infty}^{t} dt' \ e^{\frac{\gamma t'}{m}} \frac{F(t')}{m}$$

$$v(t) = \int_{-\infty}^{t} dt' \ e^{\frac{-\gamma(t-t')}{m}} \frac{F(t')}{m},$$

where $e^{\frac{-\gamma t}{m}}$ plays the role of a response function. We can then calculate the autocorrelation

$$\langle v(t)v(0)\rangle = \int_{-\infty}^{t} dt_1 \int_{-\infty}^{0} dt_2 \ e^{\frac{t-t_1-t_2}{m}} \frac{\langle F(t_1)F(t_2)\rangle}{m^2}$$

$$= \int_{-\infty}^{t} dt_1 \int_{-\infty}^{0} dt_2 \ e^{\frac{t-t_1-t_2}{m}} \frac{a\delta(t_1-t_2)}{m^2}$$

$$= \int_{-\infty}^{0} dt_2 \ e^{\frac{t-2t_2}{m}} \frac{a}{m^2} = \frac{a}{2m\gamma} e^{-\frac{\gamma t}{m}},$$

where we used Eq. (2.14) and the fact that the integration commutes with the average (we are allowed to flip the order). By comparing this with the equipartition theorem we get

$$\frac{1}{2}m\langle v^2\rangle = \frac{k_BT}{2}$$

$$\frac{1}{2}m\langle v(0)v(0)\rangle = \frac{a}{4\gamma} = \frac{k_BT}{2}$$

$$a = 2\gamma k_BT$$

We notice the appearance of γ meaning that the magnitude of the fluctuations increase both with friction and temperature. Further we can integrate the velocity over time to get displacement x(t) and show that the variance (show this? In appendix maybe?) is

$$\langle x^2(t) \rangle = \frac{2k_BT}{\gamma} \left(t - \frac{m}{\gamma} \left(1 - e^{-\gamma t/m} \right) \right),$$

where for $t \gg m/\gamma$ only the t-term survies yielding

$$\langle x^2(t)\rangle = 2k_BTt/\gamma.$$

In 1D, the diffusion constant D is related to the variance as $\langle x^2 \rangle = 2Dt$, meaning that this represents the einstein relation $D = \mu k_B T$ with the mobility $\mu = 1/\gamma$.

when $t \ll m/\gamma$ we use the Taylor expansion $1 - e^{-x} \approx x - x^2/2$ for $x \ll 1$ to get

$$\left\langle x^2(t)\right\rangle = \frac{k_B T}{m} t^2$$

which exactly mathces the thermal velocity

$$v_{\rm th} \frac{\left\langle x^2(t) \right\rangle}{t^2} = \frac{k_B T}{m}$$

which follows from the equipartition theorem. The finite correlation time γ/m hence describe the crossover from the ballistic regime $\sqrt{\langle x^2(t) \rangle} \propto t$ to the diffusive regime $\sqrt{\langle x^2(t) \rangle} \propto \sqrt{t}$.

Introduce the fluctuation-dissipation theorem concept earlier since this is a motivaiton for the Langeivn equation.

2.3.2 Implementing Langevin

The implementation of the Langevin equation into LAMMPS follows [30] and updates the force vector for each particle as

$$\mathbf{F} = \mathbf{F_c} + \mathbf{F}_f + \mathbf{F}_r$$

$$= -\nabla U - \gamma m \mathbf{v} + \sqrt{\frac{2k_B T m \gamma}{\Delta t}} \mathbf{h}(t)$$
(2.15)

where $\mathbf{F_c}$ is the conservative force computed via the usual inter-particle interactions described by the potential U, \mathbf{F}_f is the drag force and \mathbf{F}_r is the random fluctuation force where \mathbf{h} is a random vector drawn from a normal distribution with zero mean and unit variance. Notice that this generalized description of the Langevin equation deviates from the presentation in Eq. (2.12) since we have added the conservative force $\mathbf{F_c}$, but also by the appearance of the mass in both the drag force and the fluctuation force due to the introduction of damping. It is beyond out scope to comprehend this. However, the fact that Δt now appears in the denomiator for the random force variance $2k_BTm\gamma/\Delta t$ is due to the fact that we have discretized time. This in agreement with the formulation in Eq. (2.13). By applying Eq. (2.15) we get the refined velocity verlet scheme

$$\begin{split} \mathbf{v}_i(t+\Delta t/2) &= \mathbf{v}_i(t) - \frac{\Delta t}{2} \left(\frac{\nabla_i U(t)}{m_i} + \gamma \mathbf{v}_i \right) + \sqrt{\frac{k_B T \gamma \Delta t}{2m_i}} \mathbf{h}_i \\ \mathbf{r}_i(t+\Delta t) &= \mathbf{r}_i(t) + \mathbf{v}_i(t+\Delta t/2) \Delta t \\ \mathbf{v}_i(t+\Delta t) &= \mathbf{v}_i(t+\Delta t/2) - \frac{\Delta t}{2} \left(\frac{\nabla_i U(t+\Delta t)}{m_i} + \gamma \mathbf{v}_i(t+\Delta t/2) \right) + \sqrt{\frac{k_B T \gamma \Delta t}{2m_i}} \mathbf{h}_i \end{split}$$

with new random vector \mathbf{h}_i for each particle and each update. Notice however, that LAMMPS only apply this scheme to the particle groups with the thermostat on.

2.4 MD limitations (?)

2.5 LAMMPS

Part II Simulations

Appendices

Appendix A

22 APPENDIX A

Appendix B

 $APPENDIX \ B$

Appendix C

APPENDIX C

Bibliography

- ¹E. Gnecco and E. Meyer, Elements of friction theory and nanotribology (Cambridge University Press, 2015).
- ²Bhusnan, "Introduction", in *Introduction to tribology* (John Wiley & Sons, Ltd, 2013) Chap. 1, 1–?
- ³H.-J. Kim and D.-E. Kim, "Nano-scale friction: a review", International Journal of Precision Engineering and Manufacturing **10**, 141–151 (2009).
- ⁴K. Holmberg and A. Erdemir, "Influence of tribology on global energy consumption, costs and emissions", Friction 5, 263–284 (2017).
- ⁵B. Bhushan, "Gecko feet: natural hairy attachment systems for smart adhesion mechanism, modeling and development of bio-inspired materials", in *Nanotribology and nanomechanics: an introduction* (Springer Berlin Heidelberg, Berlin, Heidelberg, 2008), pp. 1073–1134.
- ⁶P. Z. Hanakata, E. D. Cubuk, D. K. Campbell, and H. S. Park, "Accelerated search and design of stretchable graphene kirigami using machine learning", Phys. Rev. Lett. **121**, 255304 (2018).
- ⁷P. Z. Hanakata, E. D. Cubuk, D. K. Campbell, and H. S. Park, "Forward and inverse design of kirigami via supervised autoencoder", Phys. Rev. Res. **2**, 042006 (2020).
- ⁸L.-K. Wan, Y.-X. Xue, J.-W. Jiang, and H. S. Park, "Machine learning accelerated search of the strongest graphene/h-bn interface with designed fracture properties", Journal of Applied Physics 133, 024302 (2023).
- ⁹Y. Mao, Q. He, and X. Zhao, "Designing complex architectured materials with generative adversarial networks", Science Advances **6**, eaaz4169 (2020).
- ¹⁰Z. Yang, C.-H. Yu, and M. J. Buehler, "Deep learning model to predict complex stress and strain fields in hierarchical composites", Science Advances 7, eabd7416 (2021).
- ¹¹A. E. Forte, P. Z. Hanakata, L. Jin, E. Zari, A. Zareei, M. C. Fernandes, L. Sumner, J. Alvarez, and K. Bertoldi, "Inverse design of inflatable soft membranes through machine learning", Advanced Functional Materials **32**, 2111610 (2022).
- ¹²S. Chen, J. Chen, X. Zhang, Z.-Y. Li, and J. Li, "Kirigami/origami: unfolding the new regime of advanced 3D microfabrication/nanofabrication with "folding", Light: Science & Applications 9, 75 (2020).
- ¹³Z. Deng, A. Smolyanitsky, Q. Li, X.-Q. Feng, and R. J. Cannara, "Adhesion-dependent negative friction coefficient on chemically modified graphite at the nanoscale", Nature Materials 11, 1032–1037 (2012).
- ¹⁴R. W. Liefferink, B. Weber, C. Coulais, and D. Bonn, "Geometric control of sliding friction", Extreme Mechanics Letters 49, 101475 (2021).
- ¹⁵Y. Dong, A. Vadakkepatt, and A. Martini, "Analytical models for atomic friction", Tribology Letters 44, 10.1007/s11249-011-9850-2 (2011).
- ¹⁶N Manini, O. M. Braun, E Tosatti, R Guerra, and A Vanossi, "Friction and nonlinear dynamics", Journal of Physics: Condensed Matter 28, 293001 (2016).
- ¹⁷B. Bhushan, "Nanotribology and nanomechanics", Wear **259**, 15th International Conference on Wear of Materials, 1–? (2005).
- ¹⁸S. Li, Q. Li, R. W. Carpick, P. Gumbsch, X. Z. Liu, X. Ding, J. Sun, and J. Li, "The evolving quality of frictional contact with graphene", Nature **539**, Number: 7630, 541–545 (2016).
- ¹⁹J. Tersoff, "New empirical approach for the structure and energy of covalent systems", Phys. Rev. B 37, 6991–7000 (1988).

28 BIBLIOGRAPHY

²⁰P. Zhu and R. Li, "Study of nanoscale friction behaviors of graphene on gold substrates using molecular dynamics", Nanoscale Research Letters 13, 34 (2018).

- ²¹Q. Zhang, D. Diao, and M. Kubo, "Nanoscratching of multi-layer graphene by molecular dynamics simulations", Tribology International 88, 85–88 (2015).
- ²²H. M. Yoon, Y. Jung, S. C. Jun, S. Kondaraju, and J. S. Lee, "Molecular dynamics simulations of nanoscale and sub-nanoscale friction behavior between graphene and a silicon tip: analysis of tip apex motion.", Nanoscale 7 14, 6295–303 (2015).
- ²³S. Corporation, Pair_style lj/cut command, (Dec. 22, 2022) https://docs.lammps.org/pair lj.html.
- ²⁴X. Wang, S. Ramírez-Hinestrosa, J. Dobnikar, and D. Frenkel, "The lennard-jones potential: when (not) to use it", Phys. Chem. Chem. Phys. **22**, 10624–10633 (2020).
- ²⁵R. Naeem, Lennard-jones potential, (Nov. 25, 2022) https://chem.libretexts.org/Bookshelves/Physical_and_Theoretical_Chemistry_Textbook_Maps/Supplemental_Modules_(Physical_and_Theoretical_Chemistry)/Physical_Properties_of_Matter/Atomic_and_Molecular_Properties/Intermolecular_Forces/Specific_Interactions/Lennard-Jones_Potential.
- ²⁶S. Corporation, *Pair_style sw command*, (Dec. 22, 2022) https://docs.lammps.org/pair_sw.html.
- ²⁷F. H. Stillinger and T. A. Weber, "Computer simulation of local order in condensed phases of silicon", Phys. Rev. B **31**, 5262–5271 (1985).
- ²⁸S. Corporation, Pair_style tersoff command, (Dec. 22, 2022) https://docs.lammps.org/pair_tersoff.html.
- ²⁹J. Tersoff, "Modeling solid-state chemistry: interatomic potentials for multicomponent systems", Phys. Rev. B **39**, 5566–5568 (1989).
- ³⁰T. Schneider and E. Stoll, "Molecular-dynamics study of a three-dimensional one-component model for distortive phase transitions", Phys. Rev. B **17**, 1302–1322 (1978).